ACCSCIENCE PUBLISHING

International Journal of Bioprinting

RESEARCH ARTICLE

Bioprinted autologous human skin equivalents for *in vitro* testing of therapeutic antibodies

Mahid Ahmed[1,2], David Hill[3,4], Shaheda Ahmed[2], Stefan Przyborski[5,6], Kenneth Dalgarno[1]*, and Anne Dickinson[2,4]

[1]School of Engineering, Newcastle University, Newcastle upon Tyne, NE3 1PS, United Kingdom

[2]Alcyomics Ltd., The Biosphere, Draymans Way, Newcastle Helix, Newcastle upon Tyne, NE4 5BX, United Kingdom

[3]Faculty of Health Sciences and Wellbeing, Sunderland University, Sunderland, SR1 3SD, United Kingdom

[4]Translational & Clinical Research Institute, Faculty of Medical Science, Medical School, Newcastle University, Newcastle upon Tyne, NE2 4HH, United Kingdom

[5]Department of Bioscience, Durham University, South Road, Durham, DH1 3LE, United Kingdom

[6]Reprocell Europe Ltd., NETPark Plexus, Thomas Wright Way, Sedgefield, Co. Durham, TS21 3FD, United Kingdom

Abstract

In recent years, advances in tissue engineering have brought forward the accessibility of human skin equivalents for *in vitro* applications; however, the availability of human-based engineered tissue models suitable for high-throughput screening of biologics remains limited. Here, we report a method of manufacturing fully autologous (with both fibroblasts and keratinocytes from the same donor) human skin equivalents for determining preclinical therapeutic antibody adverse immune reactions *in vitro*. Using a combination of precise solenoid microvalve-based bioprinting and 96-well scale Alvetex inserts, autologous skin cells were bioprinted and cultured to develop a scalable approach to manufacturing skin equivalents. We demonstrated that fibroblasts and keratinocytes can be bioprinted with a high degree of precision while maintaining viability post printing. Histological staining showed that the bioprinted 96-well based skin equivalents were comparable to human skin. The fully autologous human skin equivalents were co-cultured *in vitro* with autologous peripheral blood monocytes with and without muromonab-CD3 (OKT3) and natalizumab (Tysabri), biologics which are known to cause and inhibit adverse immune reactions (type IV hypersensitivity), respectively. Analysis of supernatants from skin-equivalent monocyte co-cultures revealed significant proinflammatory cytokine responses (such as interferon gamma) in co-cultures treated with OKT3 when compared to Tysabri and negative controls. Consequently, this study provides proof of concept that through a combination of bioprinting and Alvetex scaffold-based culture systems, scalable human skin equivalents can be manufactured for high-throughput identification of adverse immune reactions during preclinical stages of the drug development process.

Keywords: Autologous tissue models; Skin-equivalent models; Microvalve bioprinting; Transwell culture

***Corresponding author:**
Kenneth Dalgarno
(kenny.dalgarno@newcastle.ac.uk)

Citation: Ahmed M, Hill D, Ahmed S, Przyborski S, Dalgarno K, Dickinson A. Bioprinted autologous human skin equivalents for *in vitro* testing of therapeutic antibodies. *Int J Bioprint*. 2024;10(2):1851. doi: 10.36922/ijb.1851

Received: September 17, 2023
Accepted: January 10, 2024
Published Online: March 11, 2024

1. Introduction

The limited availability of human tissue for preclinical assays compounds the need for the use of animal-based studies during the drug development process. In addition to the ethical concerns associated with the use of animal models, such studies may not be representative of the outcome of subsequent first in human studies.[1] This contributes to the high failure rate that the pharmaceutical industry experiences when taking drugs to human clinical trials.[2] *In vivo* animal models ultimately differ in physiology to humans.[3] Even in the case of larger animal models such as non-human primates, many underlying differences remain, influencing the efficacy of animal models as pre-clinical tools.[3] When adverse immune reactions (which may cause type IV hypersensitivity reactions) of a drug are not identified in preclinical studies but become apparent during clinical trials, the consequences for participants can be seriously life-threatening.[1,4] Furthermore, the financial burden resulted from clinical trial failure may further hinder drug developers.[5] With high rates of failure at clinic and a reported decline in both pharmaceutical research and development productivity and investment,[6] the mantra of "fail early, fail fast" is becoming increasingly important to drug developers.

Following the signing of the FDA Modernization Act 2.0, drug developers are under increasing pressure to investigate the use of non-animal-based assays. While *in vitro* and *ex vivo* assays are used during the preclinical development process,[7] there is a growing need for tools that can provide greater physiologically relevant complexity and interactions. *Ex vivo* assays can be used to determine adverse immune responses to systemic therapies.[8] However, human-based *ex vivo* assays that seek to bridge the gap between preclinical animal studies and human clinical trials are challenging to scale up. Looking beyond the scope of drug development, access to human tissue remains a barrier even for medical and biological research.[9] With an overall movement toward the 3Rs (Reduction, Refinement, and Replacement), there is growing interest, however, in human *in vitro* three-dimensional (3D) models.

In recent years, the fields of *in vitro* tissue engineering and 3D cell culture have benefited from the growth of biofabrication techniques.[10,11] Within the tissue engineering community, biofabrication is considered to be the intersection of additive manufacturing, the layer-by-layer process of manufacturing a 3D construct, and tissue engineering.[12] To biofabricate tissue constructs, bioprinting is commonly used to organize and print cells or cell aggregates to create a 3D tissue model.[11] Bioprinting itself can be categorized into four commonly used methods: extrusion-based bioprinting and three drop-on-demand (DoD) processes inkjet printing, microvalve bioprinting, and laser-based bioprinting. Extrusion-based bioprinting uses pneumatic or mechanical mechanisms, allowing close control of bioink[13] material flow, making the process ideal for the deposition of pre-mixed hydrogels.[14,15] Inkjet bioprinting is DoD process, which typically uses thermal actuators[16] or piezoelectric actuators[17] to dispense individual droplets of bioink in the picoliter range.[18] This makes inkjet printing ideal for low-viscosity bioinks with lower cell densities.[15] Laser-based systems use the principle of laser-induced forward transfer to dispense individual droplets of material, which are typically cell-laden hydrogels.[13] Like inkjet bioprinters, microvalve bioprinters dispense low-viscosity bioinks, but it has also been demonstrated that microvalves can be arranged in a print-head such that they can print materials such as hydrogel precursors laden with a high density of cells.[19] For low-viscosity bioinks, microvalve can deposit high droplets of high-cell-concentration solutions in the nanoliter range,[20] and so for the development of micro-tissue models offers an efficient way of depositing the numbers of cells that such models require.

The bottom-up nature of biofabrication has led to the production of a range of engineered tissue-like constructs or scaffolds suitable for tissue engineering such as skin equivalents, constructs for bone repair, cartilage-like tissue, and cardiac models.[21-24] However, these examples typically rely on allogeneic materials to create 3D tissue constructs. Examples of bioprinted tissues where autologous cells and autologous materials are applied largely fall within the scope of regenerative medicine.[25,26] In contrast, it has been demonstrated that using traditional top-down approaches to tissue engineering can produce fully humanized constructs, which may be adapted to autologous settings.[27] In particular, the use of inert permeable plastic scaffolds with porous substrates, such as Transwell® and Alvetex® scaffolds, has become almost ubiquitous as the method of creating bi-layered keratinocyte-fibroblast co-cultures for skin equivalents.[28] However, traditional approaches to tissue engineering lack the benefit of automation and therefore the scalability offered by biofabrication. In considering scalability, the use of standard well-plate formats is a key enabler as it allows for scale up and scale out in a format familiar in most microbiology labs and which is easy to interface with many downstream processes. As such, there is limited availability of scalable, fully humanized and autologous tissue available for preclinical *in vitro* drug screening.

Here, we demonstrate how the permeable scaffold approach can be combined with microvalve-based biofabrication to develop a fully human, autologous skin equivalent which can be co-cultured with autologous immune cells in a 96-well format. This approach provides

proof-of-concept that human skin equivalents produced, using scalable, automated biofabrication techniques can be used as a preclinical tool to predict potential adverse immune responses of therapeutic antibodies.

2. Materials and methods

2.1. Cell culture

Full Local Research Ethics Committee (LREC) approval was obtained before sourcing healthy volunteer samples for this study. After obtaining informed consent, two 4 mm skin biopsies and 60 mL of whole blood were collected from healthy volunteers. Skin biopsies were rinsed in phosphate-buffered saline (PBS; Sigma-Aldrich, UK), then excess adipose tissue was removed from the skin biopsies, and the biopsies were incubated in 1.0 U/mL dispase solution (Scientific Laboratory Supplies, UK) for 18 h at 4°C to allow separation of the epidermis from the dermis. Once separated, the dermis and epidermis were processed independently. To isolate dermal fibroblasts, the separated dermal samples were dissected, placed into 6-well plates, and covered with 100 µL of fetal bovine serum (FBS; Thermo Fisher Scientific, UK). The dermal samples were incubated using standard culture conditions (37°C with 5% CO_2) for 24 h. After 24 h, wells were topped up with 5 mL of Media A (Table 1). Dermal dissects were observed for fibroblast outgrowth with media changed twice weekly. Once significant outgrowth was observed, fibroblasts were dissociated using trypsin/EDTA (Sigma-Aldrich) using standard culture conditions for 5 min. The dissociated fibroblasts were further cultured for up to 7 passages. Keratinocytes were dissociated from epidermal samples using trypsin/EDTA using standard cell culture conditions. The resulting cells were further cultured in Media B (Table 1) for up to 3 passages with media changed twice weekly. Lymphoprep™ density gradient medium (STEMCELL Technologies, UK) was used to isolate human peripheral blood monocytes (PBMCs) from whole blood sourced from healthy volunteers as previously described.[8]

2.2. Bioprinting equipment and process

For this study, a Microfab Jetlab 4 XL (Microfab Technologies Inc., US) printer was retrofitted to accommodate solenoid VHS series microvalves (Lee Products Ltd., US)

Table 1. Media formulations and working concentrations

Media	Components	Supplier	Final concentration
A	Dulbecco's Modified Eagles Medium	Sigma-Aldrich, UK	-
	Fetal calf serum	Fisher Scientific, UK	10%
	Penicillin/Streptomycin/Amphotericin	Sigma-Aldrich, UK	1%
	L-glutamine	Sigma-Aldrich, UK	1%
B	Epilife	Fisher Scientific, UK	-
	Human Keratinocyte Growth Supplement	Fisher Scientific, UK	1%
	Penicillin/Streptomycin/Amphotericin	Sigma-Aldrich, UK	1%
	L-glutamine	Sigma-Aldrich, UK	1%
C	3 Part Dulbecco's Modified Eagles Medium	Sigma-Aldrich, UK	-
	1 Part Ham's F12 Nutrient Mixture	Sigma-Aldrich, UK	-
	Chelex-treated fetal calf serum	Fisher Scientific, UK	5%
	Penicillin/Streptomycin/Amphotericin	Sigma-Aldrich, UK	1%
	L-glutamine	Sigma-Aldrich, UK	1%
	Cholera toxin	Sigma-Aldrich, UK	8.5 ng/mL
	Hydrocortisone	Sigma-Aldrich, UK	0.4 µg/mL
	Human insulin	Sigma-Aldrich, UK	5 µg/mL
	Adenine	Sigma-Aldrich, UK	24 µg/mL
	Human epidermal growth factor	PeproTech, US	20 ng/mL
D	3 Part Dulbecco's Modified Eagles Medium	Sigma-Aldrich, UK	-
	1 Part Ham's F12 Nutrient Mixture	Sigma-Aldrich, UK	-
	Fetal calf serum	Fisher Scientific, UK	10%
	Penicillin/Streptomycin/Amphotericin	Sigma-Aldrich, UK	1%
	Cholera toxin	Sigma-Aldrich, UK	8.5 ng/mL
	Hydrocortisone	Sigma-Aldrich, UK	0.4 µg/mL
	Human epidermal growth factor	PeproTech, US	20 ng/mL
	Human transferrin	PeproTech, US	5 µg/mL
	L-ascorbic acid	Sigma-Aldrich, UK	100 µg/mL
F	RPMI-1640	Sigma-Aldrich, UK	-
	Autologous serum	-	20%
	Penicillin/Streptomycin/Amphotericin	Sigma-Aldrich, UK	1%

to create a high-throughput bioprinting platform. The inkjet printhead of the Jetlab 4 printer was replaced with a microvalve printhead (Figure 1), which could accommodate four individual custom-built ink reservoirs, each with an ink capacity of 2.5 mL. Inkjet printing is very effective for small volumes and can offer single-cell resolution, but the development of skin-equivalent models requires higher volume deposition rates, and so, for this reason, microvalve printing was preferred. The outlets of the reservoirs were threaded to contain a male–male 062 MINSTAC threaded connector (Lee Products Ltd.); one side of which was fixed into the reservoir (Figure 1). The other end of the male–male connector was used to attach the solenoid VHS series. The valve configuration used in this study had female 062 MINSTAC threaded inlets and outlets and was used alongside 062 MINSTAC jeweled orifice nozzles (Lee Products Ltd., US) with orifice diameters of 190 µm. To generate actuation signals for the microvalves, spike and hold electrical drivers (Lee Products Ltd.) were connected to both the Jetlab 4 device signal output channels and the signal connections of the Individual valves. This allowed signals produced by the waveform printed circuit board (PCB) of the Jetlab to be converted to a 24 V spike voltage and a 5 V dwell voltage. The optimal parameters for reliable microdispensing of low viscosity inks were investigated by exploring the impact on adjusting the operating dwell time (time that the microvalve remains open during one actuation cycle) and pneumatic backpressure used to eject droplets from the reservoir. The custom-designed reservoir housed a gold-plated neodymium magnet, which was suspended within the bioink and was used to agitate cells within the bioink. The magnet within the reservoir was rotated by an additional rotating magnet located perpendicular to the external wall of the reservoir. The external magnet was connected to a 24 V DC motor via drive belt, which was operated at 18 V for printing of cells. To measure the volume dispensed, 200 droplets of media D (Table 1) were printed into 1.5 mL Eppendorf tubes (Fisher Scientific), which was weighed using a microbalance (Mettler Toledo). The volume per droplet was calculated from this data. Dwell times of 100–1000 µs and backpressures of 50–500 mmHg were investigated at increments of 50 µs and 50 mmHg. To further ensure consistency of output, a microvalve purge step was used between print events.

2.3. Cell viability post printing

To ensure that the correct number of dermal fibroblasts and epidermal keratinocytes were dispensed when printing skin equivalents, fibroblast suspensions were prepared at a concentration of 25×10^6 cells/mL in Media A and keratinocytes were prepared at a concentration of 20×10^6 cells/mL in Media B and loaded into reservoirs. Following a 60 µL purge of the bioink through the microvalves, 20 µL of each cell suspension was printed in three separate wells of a 96-well plate. Cells were printed with a backpressure of 150 mmHg and a dwell time of 1000 µs. As described above, a 10 µL aliquot of each printed suspension was then mixed 1:1 with trypan blue, and cell number and viability were quantified using a hemocytometer.

2.4. Bioprinting of cells for the development of autologous skin equivalents

Figure 2 illustrates the 96-well Alvetex® (Reprocell, UK) culture system, and the general approach to developing

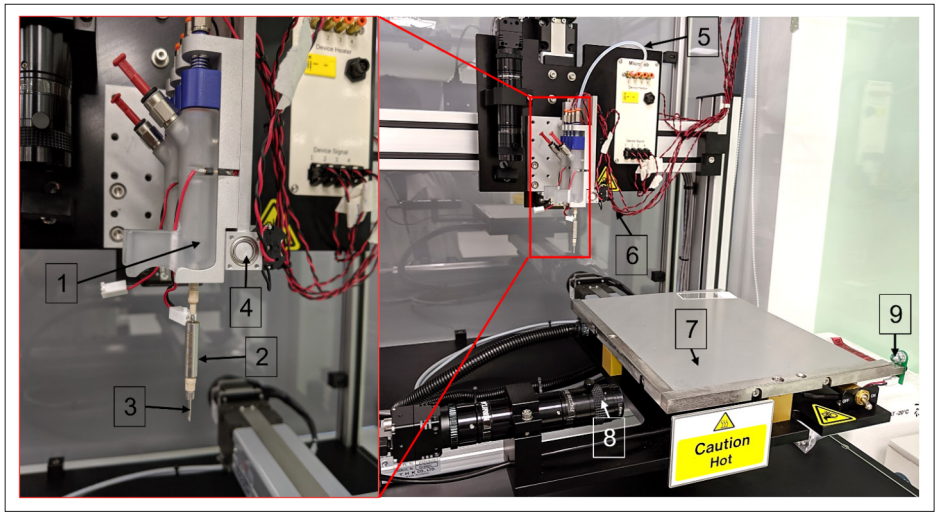

Figure 1. Customized Jetlab bioprinter. (1) Ink reservoir which holds the bioink and magnet to agitate cell suspension. (2) Solenoid valve. (3) Removable nozzle. (4) Magnetic agitator to rotate the gold-plated magnet present within the reservoir. (5) Backpressure tubing. (6) Valve actuation signal wiring. (7) XY printing platform. (8) Drop analysis camera. (9) Stroboscopic LED.

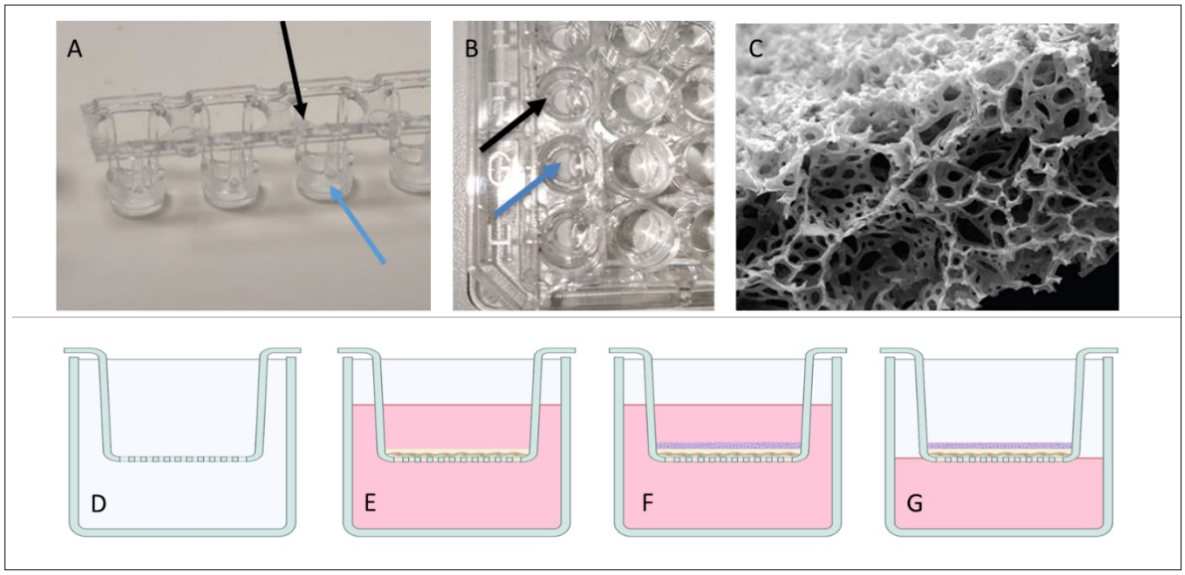

Figure 2. Development of skin equivalent models. (A, B) 96-well Alvetex® scaffold system; black arrows show inserts, blue arrows porous membrane. (C) 200 µm thick Alvetex® porous membrane. (D–G) Stages in model development. (D) Schematic of scaffold insert. (E) Dermal incubation of fibroblasts only for up to 28 days. (F) Basal incubation of keratinocytes for 3 days. (G) Incubation of model at air–liquid interface for 14 days. Panels D–G were created using Biorender.com.

skin equivalents. Prior to printing of cells, the 96-well Alvetex® (Reprocell, UK) scaffolds were washed in 70% ethanol and rinsed in two changes of PBS. A fibroblast cell suspension was prepared in Media A at a concentration of 25×10^6 cells/mL. The Suspension (20 µL) was directly printed onto the Alvetex® scaffolds within the Transwells to create dermal equivalents, which were then incubated at standard culture conditions for 3 h. Following the 3-h incubation, the cell-laden scaffolds were submerged in Media A overnight. After 24 h, the scaffolds were cultured using Media A supplemented with 100 µg/mL of L-ascorbic acid. The dermal equivalents were cultured for 18 days with media changed daily. After 18 days, the dermal equivalents were gently rinsed in PBS to remove excess media prior to directly printing the autologous epidermal keratinocytes on top of the dermal equivalents. Keratinocytes were suspended in Media C (Table 1) at a concentration of 20×10^6 cells/mL with 20 µL of the keratinocyte cell suspension printed onto each dermal equivalent. The co-cultures were then incubated for 90 min at standard culture conditions and then gently submerged in Media C for 3 days with media changed daily. Skin equivalents were then raised to the air–liquid interface (ALI) by aspirating Media C and adding sufficient Media D (Table 1) to the wells to cover the underside of each dermis, without submerging the epidermis region of the tissue. The co-cultures were cultured at the ALI at standard conditions for 14 days with media changed daily. After day 14 of ALI culture, the skin equivalents were harvested for histological evaluation or further cultured with autologous immune cells and monoclonal antibodies.

2.5. Histological evaluation of skin equivalents

Mature skin equivalents were harvested, formalin-fixed, paraffin-embedded, and sectioned. Sections (4 µm) were stained with hematoxylin and eosin (H&E; Fisher Scientific, UK) and Picrosirius red (Abcam, UK). Skin equivalents were analyzed for specific biomarkers, cytokeratin, involucrin, and loricrin via immunofluorescence. Sections were taken to water, washed in pH 7.4 tris-buffered saline (TBS), and antigen retrieval was conducted using pH 6 citrate buffer for 10 min. Sections were washed in TBS and then permeabilized with 0.2% Triton-X for 10 min followed by blocking with 10% goat serum (Sigma-Aldrich, UK) for 1 h. Sections were washed in TBS and then incubated with primary antibodies prepared in 10% goat serum for 1 h. Primary antibodies used were mouse anti-cytokeratin 14 (1:250, ab7800, Abcam), rabbit anti-involucrin (1:400, ab181980, Abcam), rabbit anti-cytokeratin 10 (1:500, ab76318, Abcam), and rabbit anti-loricrin (1:125, ab198994, Abcam). After 1 h, sections were washed in TBS and then incubated with secondary antibodies goat anti-mouse Alexa Fluor-488 (AF-488; Thermo Fisher Scientific) and goat anti-rabbit Alexa Fluor-647 (AF-647; Thermo Fisher Scientific); dilution of 1:400 was used for both. Slides were rinsed in a final wash of TBS, and then coverslips were mounted with Vectashield® mounting medium with DAPI (Vector Laboratories, US). Slides were imaged using an Axioimager microscope (Carl Zeiss AG, Germany).

2.6. Assessment of adverse immune reactions of monoclonal antibodies

Fully developed and autologous bioprinted skin equivalents were washed twice with PBS before co-culture with autologous PBMCs in 96-well plates with 1×10^6 cells per well in Media E (Table 1). Skin equivalents were treated with 1 μg/mL of OKT3 (Jannsen-Cilag, UK) or Tysabri (Biogen Idec Inc., US). Negative controls were skin equivalents cultured in Media E with and without autologous PBMCs and without biologics. The co-cultures were incubated at standard culture conditions for 3 days when 100 μL of supernatant was aspirated to analyze proinflammatory cytokine release.

2.7. Multiplex proinflammatory cytokine detection assay

To quantify cytokine secretion in supernatants of autologous skin-equivalent PBMC co-cultures, a multiplex human proinflammatory cytokine panel kit (Meso Scale Discovery, US) for identification of interferon gamma (IFN-γ), interleukin-10 (IL-10), interleukin-12 p70 (IL-12p70A), interleukin-13 (IL-13), interleukin-1 beta (IL-1β), interleukin-2 (IL-2), interleukin-4 (IL-4), interleukin-6 (IL6), and tumor necrosis factor alpha (TNFα) was used as per manufacturer instructions with the omission of IL-8 detection antibodies. Plates were analyzed using a QuickPlex multiplex plate reader (MSD). Supernatants were analyzed in biological triplicates.

2.8. Statistical analysis

Data are presented as mean ± standard deviation. Statistical analyses for the quantified cytokine levels were conducted using one-way analysis of variance (ANOVA) with Tukey HSD. Parameters for statistical significance were defined as $p \leq 0.05$ (*) and $p \leq 0.0001$ (****).

3. Results

3.1. Printing parameter optimization and printing of skin cells

Optimal printing parameters were established by characterizing changes in printing dwell time and backpressure and measuring the dispensed volumes, as shown in Figure 3. Figure 3 shows that a minimum dwell time of 200 μs and backpressure of 50 mmHg could

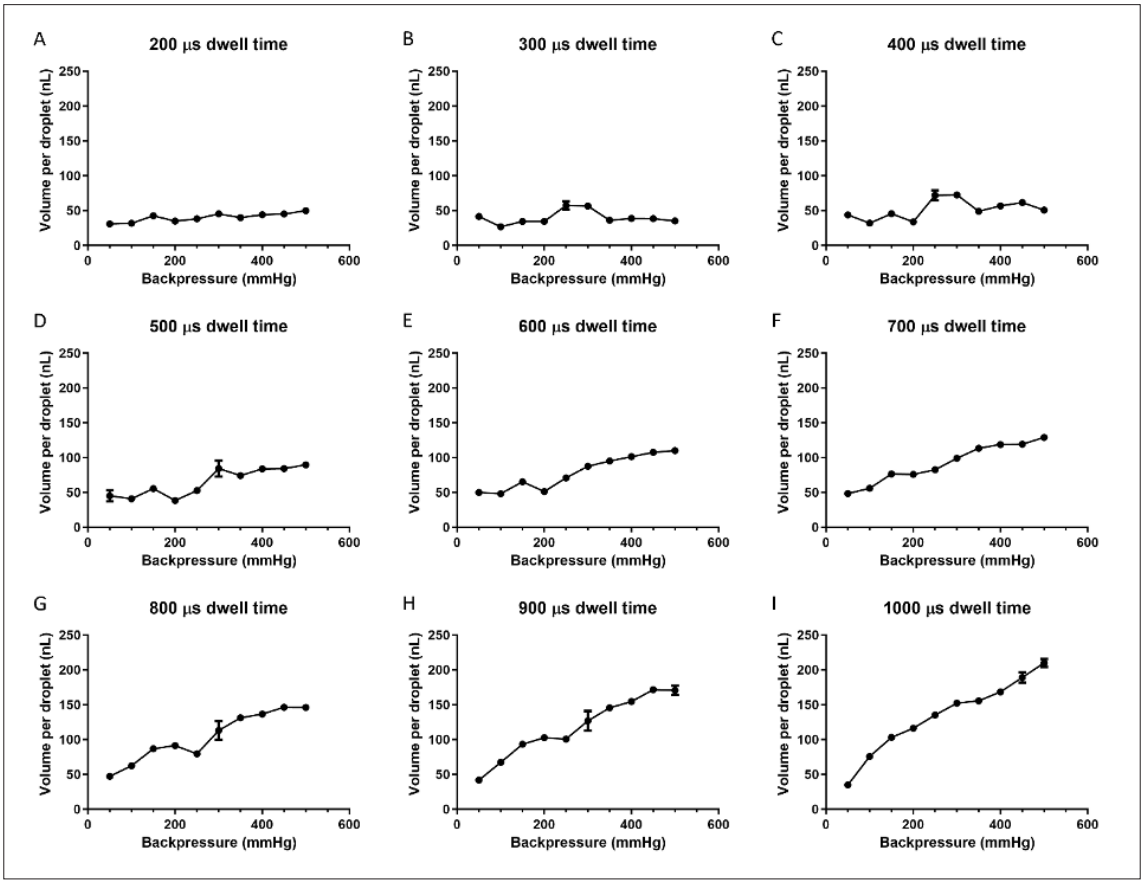

Figure 3. Mean volume of media dispensed per droplet at varying dwell times and positive pneumatic pressures. Data are presented as mean ± one standard deviation. $N = 3$.

successfully deposit material, and attempting to print with parameters below these values did not yield successful droplet deposition. At lower dwell times (Figure 3A–D), a variance in the volume per droplet was demonstrated across the range of backpressures tested. Higher dwell times (Figure 3E–I) resulted in a more linear increase in the volume per droplet dispensed across the pressure range. Peak output was 210 ± 6 nL per droplet, produced at a dwell time of 1000 µs with a backpressure of 500 mmHg. A dwell time of 1000 µs and a backpressure of 150 mmHg with a volume per droplet of 103 ± 1 nL were used to print cells and produce skin equivalents, giving good balance between productivity and consistency of output.

To print the skin-equivalent models, fibroblasts were suspended at 25 × 10^6 cells/mL and keratinocytes were suspended at 20 × 10^6 cells/mL with 20 µL of each suspension per well into 3 wells. The cell counts and viability from bioprinting of both fibroblasts and keratinocytes are presented in Figure 4. Both the number and viability of printed cells were stable and consistent across both cell types, demonstrating that the bioprinter was robust and reproducible in dispensing high number of cells within a small volume.

3.2. Histology of bioprinted skin

Representative images of H&E-stained bioprinted dermal and full-thickness skin equivalents are shown in Figure 5, with human skin shown in Figure 5D for reference. Figure 5A shows a good distribution of cells throughout the scaffold, with a consistent layer of dermal fibroblasts seen lining the top surface of the scaffold. Within the scaffold, clusters of cells could be seen near the upper surface of the scaffold, but the number of cells within the scaffold increased toward the bottom of the scaffold. Underneath the scaffold, a thick fibroblast layer was visible. Fibers of eosin-stained extracellular matrix (ECM) produced by the fibroblasts were also observed. An H&E-stained full-thickness skin equivalent can be seen in Figure 5B. The dermis of the full-thickness human skin equivalent (HSE) was well populated with a layer of fibroblasts on top of the scaffold supporting the epidermis. The epidermis of the HSE contained visible basal, spinous, and granular layers and a very thin stratum corneum. The differentiating and superficially migrating keratinocytes formed a spinous layer. The layer of granular cells indicated by the darker and slightly speckled hematoxylin-stained nuclei (which separated during sectioning) was located above the spinous keratinocytes. Picrosirius red staining of bioprinted full-thickness skin equivalents showed that the dermis was heavily loaded with collagen (Figure 5C). Large thick crosslinked collagen layers could be seen directly beneath the epidermis at the dermal–epidermal junction. This layer of collagen could be seen across the dermis, supporting the formation of an epidermis.

Immunofluorescence staining was used to stain markers present throughout the different layers in the epidermis of both healthy human skin and bioprinted full-thickness skin equivalents (Figure 6). Cytokeratin 14 (CK14) was detected directly above the dermal–epidermal junction (white dotted line), indicating the presence of basal keratinocytes at the dermal epidermal junction. The basal keratinocytes superficially migrated, stratified, and expressed cytokeratin 10 (CK10) when undergoing differentiation. CK10 was positively detected above basal keratinocytes indicating stratification and the formation of a spinous strata. Involucrin was expressed in the same regions as CK10, and loricrin was present in the corneal envelope of the epidermis. Overall, the bioprinted full-thickness skin equivalents featured the relevant epidermal differentiation markers within the correct regions of the epidermis showing that the skin equivalents were comparable to healthy human skin.

Quantified levels of proinflammatory cytokines are presented in Figure 7. The elevated IL-2 levels in specimens treated with OKT3 (muromonab) were significant when

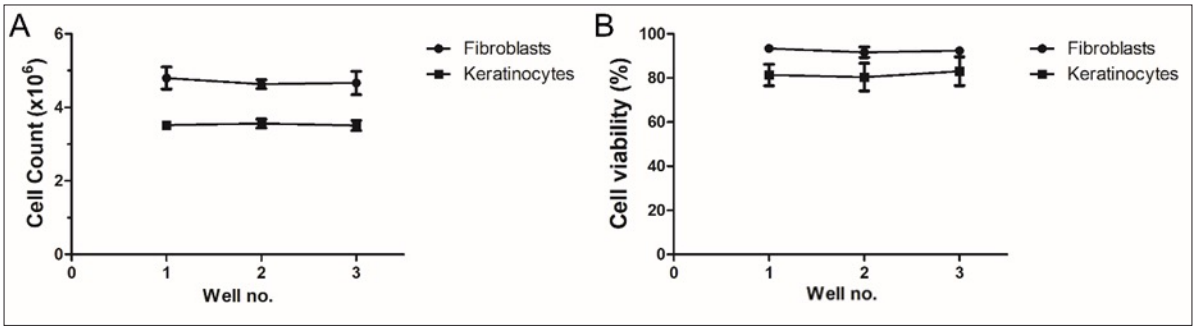

Figure 4. Cell counts and viability of both bioprinted fibroblasts and keratinocytes under a dwell time 1000 µs and backpressure of 150 mmHg. (A) Cell counts of bioprinted fibroblasts and keratinocytes. (B) Cell viability of fibroblasts and keratinocytes. Data are presented as mean ± one standard deviation. $N = 3$.

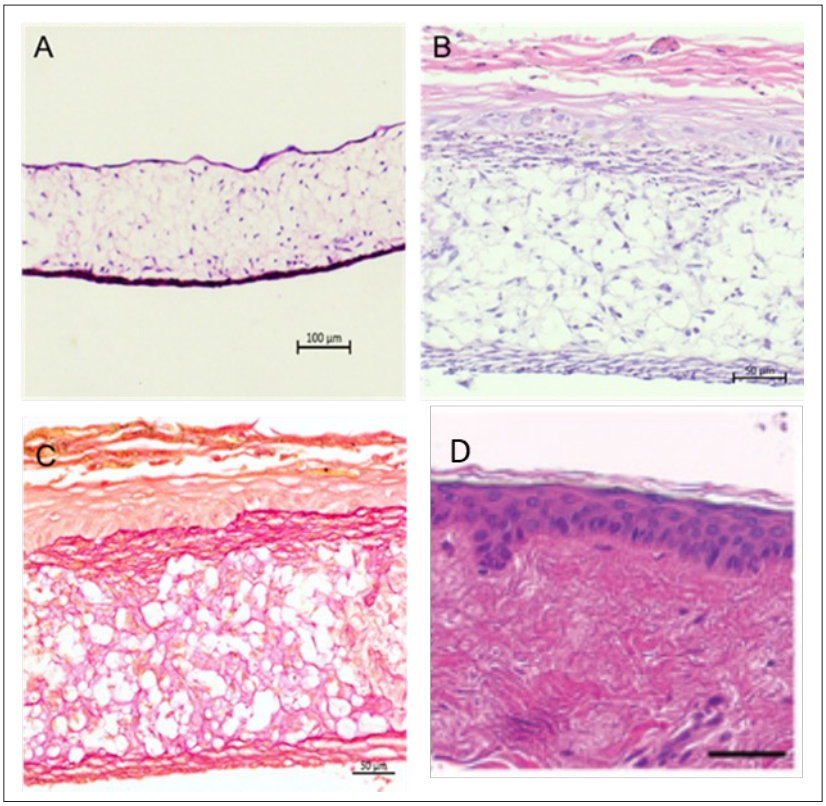

Figure 5. Representative staining of bioprinted dermal and full-thickness skin equivalents. (A) Representative H&E staining of dermal equivalent (day 14); scale bar: 100 µm. (B) Representative H&E staining of full-thickness skin equivalent (day 35); scale bar: 50 µm. (C) Representative Picrosirius red staining of full-thickness skin equivalents (day 35); scale bar: 50 µm. (D) H&E staining of human skin, scale bar 25 µm.

compared to the media and isotype controls, suggesting an OKT3-induced T-cell response. This links to IFN-γ expression in OKT3-treated co-cultures, where T cells activated by IL-2 could then increase expression of IFN-γ. There was no statistical significance in secretion of both IL-4 and IL-13. IL-4 and IL-13 are both associated with a Th2 type response,[29,30] and the lack of expression of IL-4 and IL-13 also suggests that a Th2 immune response was not induced. The elevated expression of TNF-α is comparable to the use of OKT3 *in vivo* while the levels of TNFα, IFN-γ, and IL-2 are similar to cytokine profiles generated *in vitro*.[31,32] All models show high levels of expression of IL-6, which is not unexpected, as it is constitutively produced by keratinocytes,[33] but no significant differences are seen for this marker across the experimental conditions. This data indicates that it is feasible to use fully humanized full-thickness bioprinted HSEs to identify the immunotoxicity of monoclonal antibodies *in vitro* by multiplex quantification of cytokines to create a cytokine profile of the potential immune response.

4. Discussion

The successful bioprinting of fully autologous skin equivalents in a 96-well format as reported in this work provides a foundation for future work to manufacture skin equivalents on an industrial scale. There have been many examples of bioprinted human skin; however, no previous studies have demonstrated that printed skin equivalents could be used for *in vitro* testing of therapeutic antibodies.[34] This novel application of a fully human bioprinted tissue suitable for *in vitro* testing of therapeutic antibodies may be highly beneficial to the drug development process of the pharmaceutical industry.[34] The proof of concept demonstrated here could be utilized during the different stages of the drug development pipeline for safety testing of drug candidates, allowing early elimination or modification of problem candidates, as well as at the preclinical stage to prevent "late failure" prior to the clinical testing phase. There have been many publications in the field of biofabrication exploring the use of DoD printing processes such as ink jetting, solenoid microvalves, and laser-assisted printing.[13,19,35] Such studies focus on the biofabrication of constructs using the deposition of high-viscosity bioinks consisting of cell-laden crosslinked gels or gel precursors.[14,20,36,37] As a result, few studies investigate the use of cell-laden low-viscosity bioinks; therefore, little information is reported on the reproducibility of the printing process. Figure 3 indicates

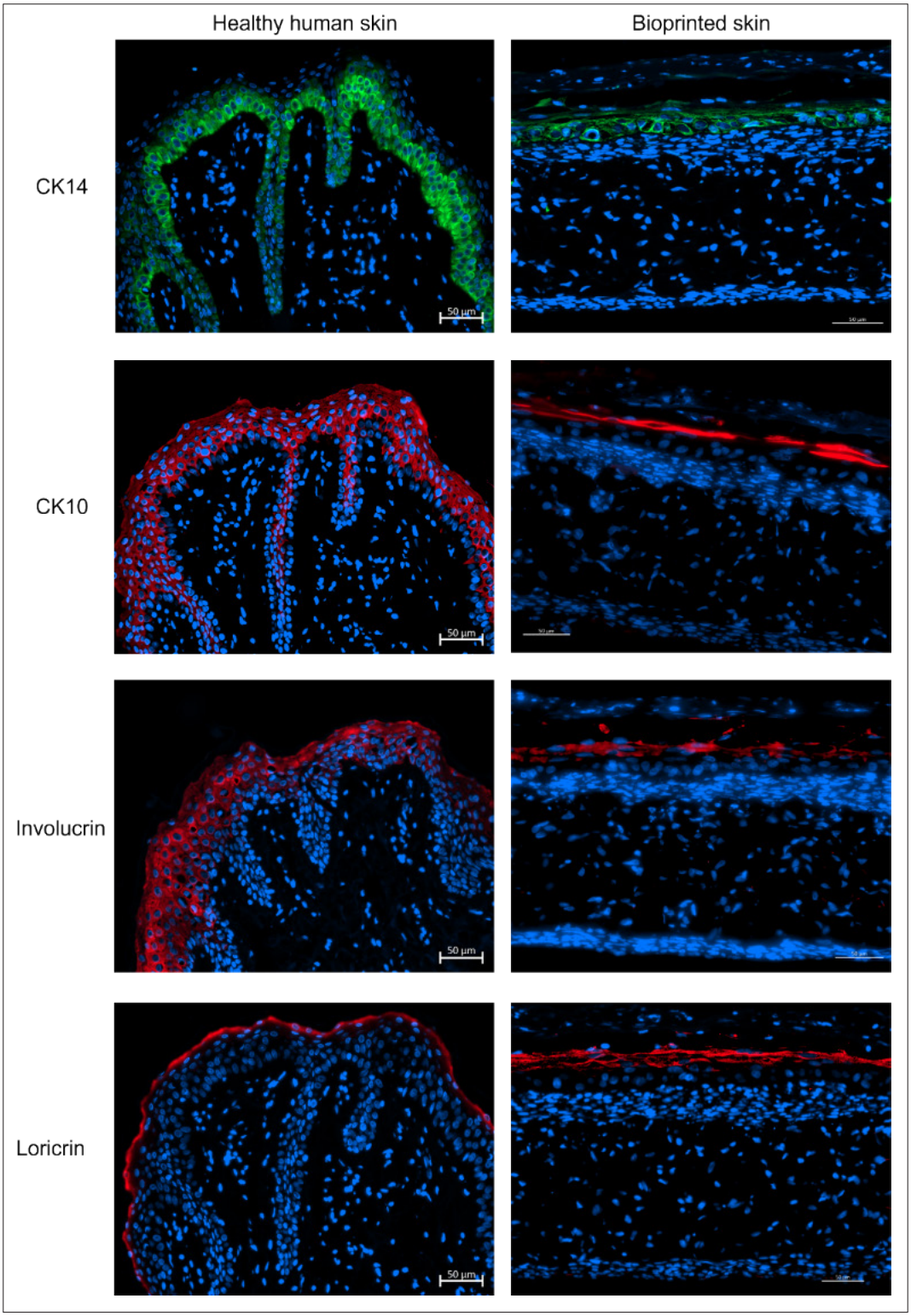

Figure 6. Representative staining of healthy human skin and bioprinted skin equivalents (at day 35). Healthy human skin and skin equivalents were stained for CK14 (green), CK10 (red), involucrin (red), and loricrin (red). Cell nuclei were stained blue with Hoechst 33342. Scale bars: 50 µm.

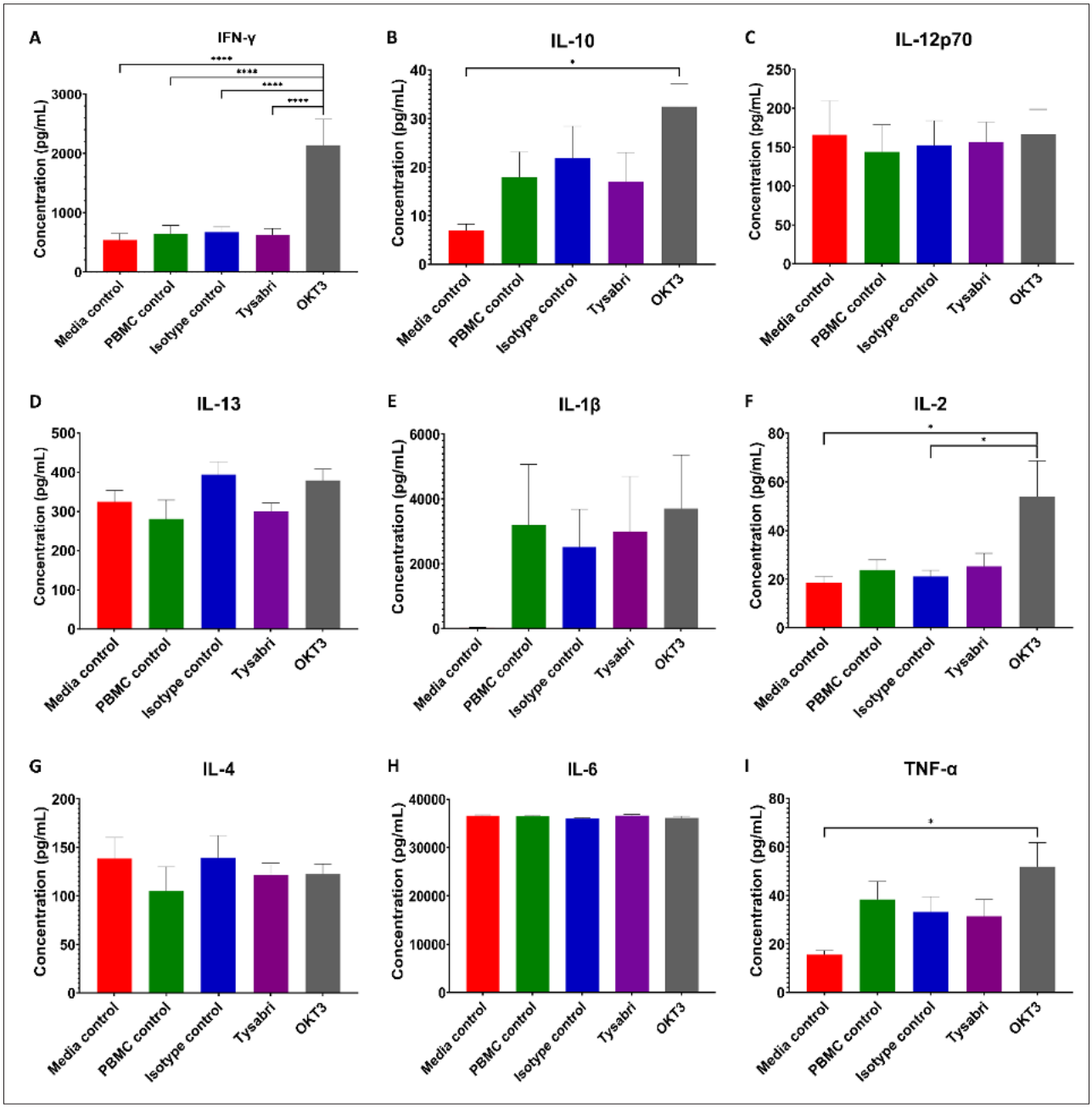

Figure 7. Mean proinflammatory cytokine concentrations from autologous co-cultures. The concentrations of cytokines detected from the supernatants of autologous co-cultures. Statistically significant differences between conditions are indicated by * and ****, which represent $p < 0.05$ and $p < 0.0001$, respectively.

that with reservoir agitation and microvalve purging, the process can offer a consistent and automatable approach in the development of tissue models.

Traditionally, commercially available skin equivalents are manufactured using top-down tissue engineering techniques. Therefore, such skin equivalents typically rely on non-human or human allogeneic ECM, as is the case for many studies which have bioprinted equivalents.[38] Therefore, currently available skin equivalents are not compatible with assays that require fully autologous systems. This work has demonstrated a hybridized approach to tissue engineering, combining top-down and bottom-up methodologies to create fully human skin equivalents. As demonstrated in this work, bioprinted skin cells can populate inert scaffolds and

produce their own ECM (Figure 5) in an autologous setting. The resulting skin equivalents were comparable to healthy human skin (Figure 6) and could be co-cultured with PBMCs to produce a fully autologous assay with automated deposition of cells, which is scalable to commercial demand. The biologically inert scaffold-based approach allows the formation of a fully autologous human skin equivalent. The bioprinting of viable and functional human cells using solenoid microvalves circumvents the labor-intensive aspect of creating 96-well tissue constructs on a large scale. This method enables the production of biologically representative and functional HSEs that may be developed in a scalable manner. This approach could potentially be applied to wider applications such as disease modeling and modeling of wound healing, and one specific aspect of future work will involve innervating the 3D skin model using neuronal and Swann cells lines in order to further validate the model and assess pain-relieving drugs. In terms of development and use of human skin equivalents, this method of biofabrication produces a human skin equivalent that provides a potential alternative to non-animal testing and avoids cross-species reactivity, which can impact data interpretation.

5. Conclusion

This study successfully demonstrated that solenoid microvalve-based bioprinting of autologous skin equivalents in a 96-well format could be used to determine adverse immune responses of monoclonal antibodies in the human setting. Primary human skin cells were shown to be viable post printing and were shown to retain the functional capabilities required of the cells to generate human skin equivalents. The co-culture of autologous bioprinted skin equivalents with autologous PBMCs successfully identified adverse immune reactions of positive and negative therapeutic antibodies, respectively. Overall, this study has demonstrated that bioprinted human tissue can identify *in vitro* adverse immune responses triggered by therapeutic antibodies. The scalability of both the Alvetex inserts and the bioprinting approach means that in combination these technologies are able to produce human skin equivalents at high-throughput rates, enhancing pre-clinical evaluation of novel biologics prior to clinical testing.

Acknowledgments

None.

Funding

This research was supported by the EPSRC Centre for Doctoral Training in Additive Manufacturing and 3D Printing (EP/L01534X/1), and by Innovate UK through Project 103597 (Novel manufacture and commercialization of a 96-well 3D skin model for drug and toxicology testing).

Conflict of interest

The authors declare no conflicts of interest.

Author contributions

Conceptualization: Kenneth Dalgarno, Anne Dickinson, Stefan Przyborski
Investigation: Mahid Ahmed
Methodology: David Hill, Shaheda Ahmed
Formal analysis: Mahid Ahmed, David Hill, Shaheda Ahmed
Writing – original draft: Mahid Ahmed, Kenneth Dalgarno, Anne Dickinson
Writing – review & editing: David Hill, Kenneth Dalgarno, Anne Dickinson, Stefan Przyborski

Ethics approval and consent to participate

Skin cells were obtained from healthy volunteers, with ethical approval for the procedure from Newcastle and North Tyne 1 Research Ethics Committee, REC 10/H0906/58.

Consent for publication

Not applicable.

Availability of data

Data can be obtained from the Newcastle University Open Data Archive (https://doi.org/10.25405/data.ncl.24566740.v1).

References

1. Stebbings R, Findlay L, Edwards C, et al. "Cytokine storm" in the phase I trial of monoclonal antibody TGN1412: better understanding the causes to improve preclinical testing of immunotherapeutics. *J Immunol.* 2007;179(5):3325-3331. doi: 10.4049/jimmunol.179.5.3325

2. Hay M, Thomas D, Craighead J, Economides C, Rosenthal J. Clinical development success rates for investigational drugs. *Nat Biotechnol.* 2014;32:40-51. doi: 10.1038/nbt.2786

3. Pound P, Ritskes-Hoitinga M. Is it possible to overcome issues of external validity in preclinical animal research? Why most animal models are bound to fail. *J Transl Med.* 2018;16:304. doi: 10.1186/s12967-018-1678-1

4. Panoskaltsis N, McCarthy NE, Knight SC. Myelopoiesis of acute inflammation: lessons from TGN1412-induced cytokine storm. *Cancer Immunol Immunother.* 2021;70:1155-1160.

doi: 10.1007/s00262-020-02702-9

5. DiMasi JA, Grabowski HG, Hansen RW. Innovation in the pharmaceutical industry: new estimates of R&D costs. *J Health Econ*. 2016;47:20-33. doi: 10.1016/j.jhealeco.2016.01.012
6. Mahlich J, Bartol A, Dheban S. Can adaptive clinical trials help to solve the productivity crisis of the pharmaceutical industry? - a scenario analysis. *Health Econ Rev.* 2021;11:4. doi: 10.1186/s13561-021-00302-6
7. Hughes JP, Rees S, Kalindjian SB, Philpott KL. Principles of early drug discovery. *Br J Pharmacol.* 2011;162(6):1239-1249. doi: 10.1111/j.1476-5381.2010.01127.x
8. Ahmed SS, Whritenour J, Ahmed MM, et al. Evaluation of a human *in vitro* skin test for predicting drug hypersensitivity reactions. *Toxicol Appl Pharmacol.* 2019;369:39-48. doi: 10.1016/j.taap.2019.02.005
9. Lawrence E, Sims J, Gander A, et al. The barriers and motivators to using human tissues for research: the views of UK-based biomedical researchers. *Biopreserv Biobank*. 2020;18(4):266-273. doi: 10.1089/bio.2019.0138
10. Harley WS, Li CC, Toombs J, et al. Advances in biofabrication techniques towards functional bioprinted heterogeneous engineered tissues: a comprehensive review. *Bioprinting.* 2021;23:e00147. doi: 10.1016/j.bprint.2021.e00147
11. di Marzio N, Eglin D, Serra T, Moroni L. Bio-Fabrication: convergence of 3D bioprinting and nano-biomaterials in tissue engineering and regenerative medicine. *Front Bioeng Biotechnol.* 2020;8. doi: 10.3389/fbioe.2020.00326
12. Groll J, Boland T, Blunk T, et al. Biofabrication: reappraising the definition of an evolving field. *Biofabrication.* 2016;8(1):013001. doi: 10.1088/1758-5090/8/1/013001
13. Koch L, Deiwick A, Franke A, et al. Laser bioprinting of human induced pluripotent stem cells-the effect of printing and biomaterials on cell survival, pluripotency, and differentiation. *Biofabrication*. 2018;10(3):035005. doi: 10.1088/1758-5090/aab981
14. Cubo N, Garcia M, Del Cañizo JF, Velasco D, Jorcano JL. 3D bioprinting of functional human skin: production and *in vivo* analysis. *Biofabrication*. 2016;9(1):015006. doi: 10.1088/1758-5090/9/1/015006
15. Murphy S, Atala A. 3D bioprinting of tissues and organs. *Nat Biotechnol.* 2014;32:773-785. doi: 10.1038/nbt.2958
16. Solis LH, Ayala Y, Portillo S, Varela-Ramirez A, Aguilera R, Boland T. Thermal inkjet bioprinting triggers the activation of the VEGF pathway in human microvascular endothelial cells *in vitro*. *Biofabrication*. 2019;11(4):045005. doi: 10.1088/1758-5090/ab25f9
17. Dudman JPR, Ferreira AM, Gentile P, et al. Reliable inkjet printing of chondrocytes and MSCs using reservoir agitation. *Biofabrication.* 2020;12(4):045024. doi: 10.1088/1758-5090/aba2f8
18. Li X, Liu B, Pei B, et al. Inkjet bioprinting of biomaterials. *Chem Rev.* 2020;120(19):10793-10833. doi: 10.1021/acs.chemrev.0c00008
19. Faulkner-Jones A, Fyfe C, Cornelissen DJ, et al. Bioprinting of human pluripotent stem cells and their directed differentiation into hepatocyte-like cells for the generation of mini-livers in 3D. *Biofabrication*. 2015;7(4):044102. doi: 10.1088/1758-5090/7/4/044102
20. Dudman J, Ferreira AM, Gentile P, Wang X, Dalgarno K. Microvalve bioprinting of MSC-chondrocyte co-cultures. *Cells*. 2021;10(12):3329. doi: 10.3390/cells10123329
21. Ng WL, Qi JTZ, Yeong WY, Naing MW. Proof-of-concept: 3D bioprinting of pigmented human skin constructs. *Biofabrication.* 2018;10(2):025005. doi: 10.1088/1758-5090/aa9e1e
22. Yang X, Lu Z, Wu H, Li W, Zheng L, Zhao J. Collagen-alginate as bioink for three-dimensional (3D) cell printing based cartilage tissue engineering. *Mater Sci Eng C*. 2018;83:195-201. doi: 10.1016/j.msec.2017.09.002
23. Fedorovich NE, Kuipers E, Gawlitta D, Dhert WJA, Alblas J. Scaffold porosity and oxygenation of printed hydrogel constructs affect functionality of embedded osteogenic progenitors. *Tissue Eng Part A*. 2011;17(19-20):2473-2486. doi: 10.1089/ten.TEA.2011.0001
24. Alonzo M, AnilKumar S, Roman B, Tasnim N, Joddar B. 3D bioprinting of cardiac tissue and cardiac stem cell therapy. *Transl Res.* 2019;211:64-83. doi: 10.1016/j.trsl.2019.04.004
25. Albanna M, Binder KW, Murphy SV, et al. In situ bioprinting of autologous skin cells accelerates wound healing of extensive excisional full-thickness wounds. *Sci Rep.* 2019;9(1):1856. doi: 10.1038/s41598-018-38366-w
26. Zhou Y, Qin R, Chen T, Zhang K, Gui J. 3D bioprinting modified autologous matrix-induced chondrogenesis (AMIC) technique for repair of cartilage defects. *Mater Des.* 2021;203. doi: 10.1016/j.matdes.2021.109621
27. Hill DS, Robinson ND, Caley MP, et al. A novel fully humanized 3D skin equivalent to model early melanoma invasion. *Mol Cancer Ther.* 2015;14(11):2665-2673. doi: 10.1158/1535-7163.MCT-15-0394
28. Choudhury S, Das A. Advances in generation of three-dimensional skin equivalents: pre-clinical studies to clinical therapies. *Cytotherapy.* 2021;23(1):P1-9. doi: 10.1016/j.jcyt.2020.10.001
29. Berger A. Th1 and Th2 responses: what are they? *BMJ*. 2000;321:424.

doi: 10.1136/bmj.321.7258.424

30. Swain SL, Weinberg AD, English M, Huston G. IL-4 directs the development of Th2-like helper effectors. *J Immunol.* 1990;145(11):3796-3806.

31. Gaston RS, Deierhoi MH, Patterson T, et al. OKT3 first-dose reaction: association with T cell subsets and cytokine release. *Kidney Int.* 1991;39(1):141-148. doi: 10.1038/ki.1991.18

32. Römer PS, Berr S, Avota E, et al. Preculture of PBMCs at high cell density increases sensitivity of T-cell responses, revealing cytokine release by CD28 superagonist TGN1412. *Blood*. 2011;118(26):6772-6782. doi: 10.1182/blood-2010-12-319780

33. Yoshizaki, K, Nishimoto N, Matsumoto K, et al. Interleukin 6 and expression of its receptor on epidermal keratinocytes. *Cytokine*. 1990;2(5):381-387. doi: 10.1016/1043-4666(90)90069-6

34. Mazzocchi A, Soker S, Skardal A. 3D bioprinting for high-throughput screening: drug screening, disease modeling, and precision medicine applications. *Appl Phys Rev.* 2019;6(1):011302. doi: 10.1063/1.5056188

35. Mandrycky C, Wang Z, Kim K, Kim DH. 3D bioprinting for engineering complex tissues. *Biotechnol Adv.* 2016;34(4): 422-434. doi: 10.1016/j.biotechadv.2015.12.011

36. Lee V, Singh G, Trasatti JP, et al. Design and fabrication of human skin by three-dimensional bioprinting. *Tissue Eng Part C*. 2014;20(6):473-484. doi: 10.1089/ten.TEC.2013.0335

37. Michael S, Sorg H, Peck CT, et al. Tissue engineered skin substitutes created by laser-assisted bioprinting form skin-like structures in the dorsal skin fold chamber in mice. *PLoS One*. 2013;8(3):e57741. doi: 10.1371/journal.pone.0057741

38. Weng T, Zhang W, Xia Y, et al. 3D bioprinting for skin tissue engineering: current status and perspectives. *J Tissue Eng.* 2021;12:20417314211028574. doi: 10.1177/20417314211028574